^{14}N and ^{2}H NMR Study of the Mesophases of Cetyltrimethylammonium Bromide in Formamide

Mika Ylihautala,[†] Juha Vaara,[†] Petri Ingman,[‡] Jukka Jokisaari,*[,†] and Peter Diehl[§]

NMR Research Group, Department of Physical Sciences, and NMR Laboratory, University of Oulu, FIN-90571 Oulu, Finland, and Department of Physics, University of Basel, CH-4056 Basel, Switzerland

Received: August 19, 1996; In Final Form: October 11, 1996[⊗]

Two mixtures of cetyltrimethylammonium bromide (CTAB) and formamide (FA), (60/40 wt % (CTAB60) and 78/22 wt % (CTAB78)), which form lyotropic mesophases, were studied by using ^{2}H and ^{14}N NMR spectroscopy at varying temperatures. Both CTAB and FA give a ^{14}N resonance, whereas the ^{2}H resonance arises from a small amount of FA-d_3 in the samples. From low to high temperature, the following phases were observed: liquid + crystal → hexagonal → isotropic and liquid + crystal → hexagonal → cubic → cubic + lamellar → lamellar for CTAB60 and CTAB78, respectively. The line shapes of the ^{2}H NMR patterns of deuterated formamide are explained with a model in which formamide is moving fast compared to its nuclear quadrupolar coupling constants in uniaxial domains oriented in different directions. For the calculation of the orientation parameters of formamide, nuclear quadrupolar coupling constants corresponding to both gas and liquid phases were utilized. The gas phase values of electric field gradient (EFG) tensors were obtained by first principles calculations applying both coupled cluster doubles and density-functional theories. The ^{14}N EFG tensor was calculated for a model of CTAB to compare the orientation of formamide and CTAB. The average location and orientation of formamide among the micelles is discussed on the basis of the best suited nuclear quadrupole coupling constants and orientation parameters.

Introduction

Cetyltrimethylammonium bromide (CTAB; $CH_3(CH_2)_{15}N(CH_3)_3Br$) is known to form micelles and lyotropic mesophases with water, formamide, and glycerol.[1,2] CTAB/formamide is a particularly suitable system for NMR studies, as all the nuclei of formamide (FA; $CHONH_2$) have NMR active isotopes. Usually spin-$^1/_2$ nuclei, ^{1}H, ^{13}C, and ^{15}N, are used. However, in the present case ^{1}H NMR spectra suffer from overlapping signals of FA and CTAB, and ^{13}C and ^{15}N NMR spectra, from the lack of sensitivity. Moreover, the information from the spectra are complex due to many dipolar couplings combined with the distribution of the angle between the external magnetic field and the director **n** of the mesophase. Instead, we have chosen to study the NMR spectra of the quadrupolar spin-1 nuclei, ^{2}H and ^{14}N, of CTAB/FA with part of FA deuterated.

Since the quadrupolar coupling is a one-spin interaction, the interpretation of the NMR spectra is relatively straightforward. An average of the interactions is observed due to molecular motions, resulting in characteristic line shapes. When the rate of molecular motion is comparable with or less than the nuclear quadrupole coupling constant (NQCC), the NMR line shape can provide information on the rate of reorientational and internal molecular motion.[3] In the fast motion limit the line shape becomes insensitive to the time scale of molecular motion. In this case the line shape depends on the average of molecular orientations.[3,4]

We report the ^{2}H (of FA-d_3) and ^{14}N (of both CTAB and FA) quadrupolar splittings as a function of temperature in two lyotropic mixtures of CTAB and FA with a small amount of FA-d_3. The phase behavior of the mixtures is identified from the data. The observed NMR line shapes in the mesophases are explained with the model of FA moving fast in uniaxial domains oriented in different directions. In addition, the orientation tensor of FA has been determined in the mesophases. For this purpose we have utilized the ^{2}H and ^{14}N NQCCs, defined as

$$\chi_i = -eQ_iF_{||}^i/h \tag{1}$$

in FA obtained from both experiment[5] and our own first principles quantum chemical calculations. In (1), eQ_i is the nuclear quadrupole moment, h is the Planck constant, and $F_{||}^i$ is the principal value of the electric field gradient (EFG) tensor

$$F_{\alpha\beta}{}^i = -\partial^2 V_i/\partial\alpha\,\partial\beta \tag{2}$$

where V_i is the electric potential at the nucleus i. Theoretical NQCCs for the deuterium and the nitrogen nuclei in FA are reported and compared with values reported in the literature. The average location and orientation of FA among the micelles is discussed on the basis of the best suited NQCCs and orientation parameters. A theoretical estimate for the ^{14}N EFG tensor of the polar head of CTAB is also given. This allows information on the orientation of the micelles to be extracted.

Methods

Sample Preparation. CTAB and FA (both of purity > 99%) were supplied by Fluka and used without further purification. Two different lyotropic mixtures were made: 60 wt % of CTAB and 40 wt % of FA (CTAB60) and another with the corresponding CTAB/FA ratio of 78/22 wt % (CTAB78). On the basis of the earlier studies,[1,2] CTAB60 and CTAB78 form hexagonal (H_α) and cubic (Q_α) mesophases, respectively, at elevated temperatures. A 5 wt % amount of FA was fully deuterated in the two samples. The samples were placed in thick wall glass tubes (o.d. = 10 mm and i.d. = 8 mm) and ca. 5 atm of xenon gas was transferred into the tubes with the aid

* Author to whom correspondence should be addressed.
[†] Department of Physical Sciences, University of Oulu.
[‡] NMR Laboratory, University of Oulu.
[§] University of Basel.
[⊗] Abstract published in *Advance ACS Abstracts,* December 1, 1996.

S1089-5647(96)02548-5 CCC: $14.00

of liquid nitrogen. Finally the tubes were sealed with a flame. Xenon was introduced because the same samples were also used in a ^{129}Xe and ^{131}Xe NMR study.[6]

NMR Experiments. The ^{2}H and ^{14}N NMR spectra were recorded on Bruker DPX400 and DRX500 spectrometers over wide temperature ranges. For ^{2}H, DPX400 operates at 61.42 MHz. A pulse length of 5.5 μs and relaxation delay of at least 0.3 s were used. For DRX500, the corresponding values were 76.77 MHz, 15 μs, and 0.65 s. For ^{14}N, only DPX400 was used with the parameters 28.90 MHz, 10 μs, and 0.2 s. On DPX400, the pulse angle was ca. 30° for both nuclei and the spectral width was chosen to cover the whole spectrum within the temperature range applied.

Temperatures were regulated on a Bruker BDTC unit, and they were calibrated by using an ethylene glycol sample. All measurements were started from the highest temperature. At each temperature at least 30 min were reserved for the stabilization. The measurements were carried out for all nuclei at one temperature, before moving to the next.

Line Shape Analysis. The ^{2}H NMR line shape analyses of the powder patterns of CTAB78 were performed on the Bruker WINFIT program based on the simplex algorithm.[7] In addition, a program using the Levenberg−Marquardt algorithm[8] for nonlinear least-squares fitting was written in the MATLAB environment for the ^{2}H NMR line shape analysis of the nonrandomly oriented CTAB60.

First Principles Calculations. Knowledge of the quadrupolar coupling tensors in the molecular frame is necessary to be able to draw information on molecular order parameters based on the observed quadrupolar splittings. Experimental estimates for the gas phase χ_N[9,10] and all the NQCCs in the liquid state[5] exist for this purpose. To obtain independent information on the quadrupolar coupling tensors in the molecular frame, EFG tensors were calculated for the ^{2}H and ^{14}N nuclei in FA using molecular orbital calculations by the Hartree−Fock (SCF) and coupled cluster doubles (CCD) wave function approaches and the density-functional theory (DFT).[11] The planar microwave geometry of Hirota *et al.*[12] was adopted, which made it possible to take advantage of the C_s point group symmetry in the calculations. The exchange-correlation functional in the DFT calculations was BPW91, where the Becke exchange[13] is used with the correlation functional by Perdew and Wang.[14] The one-particle basis used was the HIV set used previously in shielding,[15] spin−spin coupling,[16] and quadrupolar coupling[17] calculations.

We also modeled the CTAB molecule by cutting its hydrophobic tail region to a shorter hydrocarbon chain of three carbons. The structure of the resulting $CH_3(CH_2)_2N(CH_3)_3Br$ fragment was optimized at the local density approximation,[18] LDA/6-311G(2d,2p) level of theory, followed by a BPW91 calculation of the ^{14}N EFG tensor. In the latter, the 6-311G-(2d,2p) basis was used for Br and the HIII set[15] for other atoms. The principal values of the EFG tensors were converted to NQCCs according to eq 1. The quadrupolar moments $Q_D = 2.860 \times 10^{-31}$ m^2 and $Q_N = 20.2 \times 10^{-31}$ m^2 tabulated by Pyykkö and Li were used.[19]

Gaussian 94 software[20] was used in all calculations. The "FineGrid" integration mesh was utilized throughout. No frozen core option was applied. We refer to the earlier publications for details of the basis sets and to our forthcoming paper[21] on the NMR parameters of FA for a more detailed account of the present calculations.

Theoretical Background. When the molecular motion is fast compared to the NQCC, the NMR frequencies of a spin-1 nucleus are given by[22]

$$\nu_i = \nu_{0i} \pm {}^{3}/_{8}\overline{\chi}_i\{3\cos^2\theta_i - 1 + \overline{\eta}_i \sin^2\theta_i \cos 2\phi_i\} \quad (3)$$

where ν_{0i} is the resonance frequency of the nucleus i. $\overline{\chi}_i$ and $\overline{\eta}_i$ are the average NQCC and the average asymmetry parameter of the quadrupolar coupling tensor, respectively. The Euler angles θ_i and ϕ_i specify the orientation of the principal axis system (PAS) of the average EFG tensor with respect to the laboratory frame. The distribution of the angles results in the characteristic line shape.

The average NQCC and asymmetry parameter can be calculated if the molecule-fixed quadrupolar coupling tensor and orientation tensor are known. In uniaxial liquid crystal phases the $\overline{\eta}_i$ vanish and $\overline{\chi}_i$ can be described with five independent orientational order parameters:

$$\overline{\chi}_i = \frac{-2eQ_i}{3h}\{[F_{zz}{}^{i} - {}^{1}/_{2}(F_{xx}{}^{i} + F_{yy}{}^{i})]S_{zz}{}^{D} + {}^{1}/_{2}(F_{xx}{}^{i} - F_{yy}{}^{i})(S_{xx}{}^{D} - S_{yy}{}^{D}) + 2F_{xy}{}^{i}S_{xy}{}^{D} + 2F_{xz}{}^{i}S_{xz}{}^{D} + 2F_{yz}{}^{i}S_{yz}{}^{D}\} \quad (4)$$

where $F_{\alpha\beta}{}^{i}$ are the elements of the EFG tensor in a molecule-fixed coordinate system ($\alpha,\beta = x,y,z$), and $S_{\alpha\beta}{}^{D}$ are the components of the traceless and symmetric Saupe orientation tensor with respect to **n**.

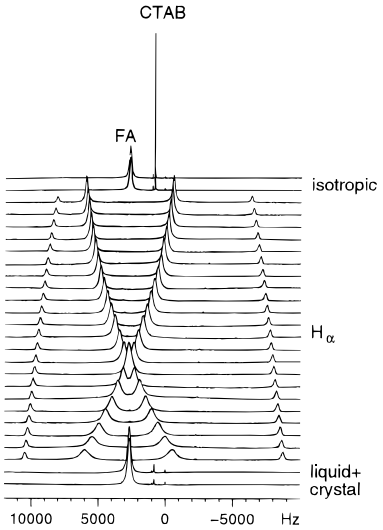

Figure 1. ^{14}N NMR spectrum of CTAB60 as a function of temperature from 313 (bottom) to 401 K (top) with a step of 3.5 K.

Results and Discussion

Phases. Figure 1 displays the stack plot of the ^{14}N NMR spectra of CTAB60 as a function of temperature. It consists of two signals: one (at low frequency) arises from the polar head of CTAB and the other (at high frequency) from FA. Three distinct phases can be seen. The middle one is clearly an oriented mesophase. The high-temperature phase (above 394 K) is an isotropic phase, where both FA and CTAB display singlets. At low temperatures (below 320 K), a liquid + crystal phase exists, in which only FA displays a clear singlet, and the CTAB signal has almost disappeared in the background due to the wide distribution of the quadrupolar splitting.

The mesophase of CTAB60 is a hexagonal H_α phase, which is also seen in the X-ray diffraction experiment.[1] The corresponding ^{14}N splitting of CTAB increases with decreasing temperature (Figure 1). If we assume that the CTAB molecule is in a cylindrically symmetric environment in the uniaxial phase

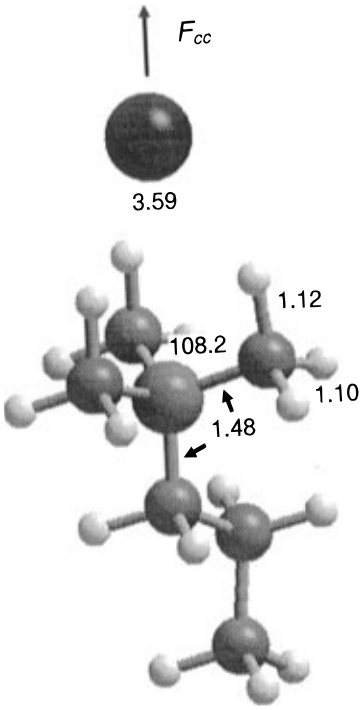

Figure 2. Optimized geometry (bond lengths in angstroms, the CNC angle in degrees) for the $CH_3(CH_2)_2N(CH_3)_3Br$ molecule for modeling CTAB. The direction of the main principal component of the ^{14}N EFG tensor is shown.

and its nonaveraged ^{14}N quadrupolar coupling tensor is cylindrically symmetric, eqs 1, 3, and 4 result in the quadrupolar splitting

$$\nu_{Q_N} = {}^3/_2\chi_N S_{cc}{}^D \tag{5}$$

where the *c*-axis points in the direction of the main principal axis of the ^{14}N NQCC (Figure 2). The experimental ^{14}N quadrupolar splitting corresponds to the parallel orientation of **n** with respect to the external magnetic field, as discussed in the section Line Shape of Formamide. Consequently, the increasing ^{14}N quadrupolar splitting of CTAB with decreasing temperature is an indication of increasing orientation $S_{cc}{}^D$ of the micelles in CTAB60 (see section Orientation).

Figure 3 shows the temperature dependence of the ^{14}N quadrupolar splittings in the CTAB60 and CTAB78 samples. An unexpected behavior is seen in the latter, where the quadrupolar splittings are visible in two distinct phases: at temperatures 334−344 and 366−394 K. On the contrary, singlets are seen within the temperature ranges 311−334 and 344−366 K. A closer look at the corresponding spectra reveals that both singlets and solidlike patterns coexist at the high-temperature region 366−380 K. This is also seen in the stack plot of the ^2H NMR spectra of CTAB78 as a function of temperature (Figure 4). At the highest temperatures almost the whole signal displays the solidlike patterns, but with decreasing temperature the proportion of singlets increases.

According to the phase diagram of Auvray *et al.*,[1] CTAB78 should exist in the cubic phase (Q_α) above 345 K and below that in the liquid + crystal phase. However, our ^2H and ^{14}N NMR measurements imply a more complex phase behavior. Again, the low-temperature phase (below 334 K) is the liquid + crystal one. CTAB78 seems to have a hexagonal phase between 334 and 344 K. The observed ^{14}N quadrupolar splittings of CTAB in the CTAB78 agree with this phase identification; the values are nearly the same as in CTAB60 (Figure 3), although the temperature evolution is opposite. In

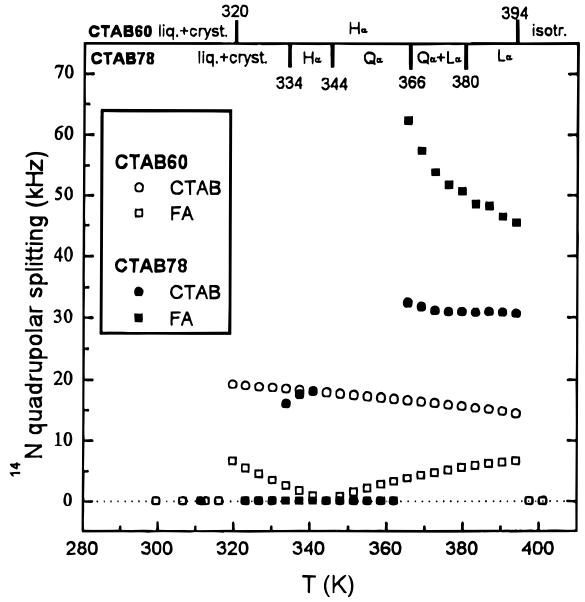

Figure 3. Absolute value of the ^{14}N quadrupolar splitting of CTAB60 and CTAB78 as a function of temperature. The phases of the samples are shown at the top of the figure.

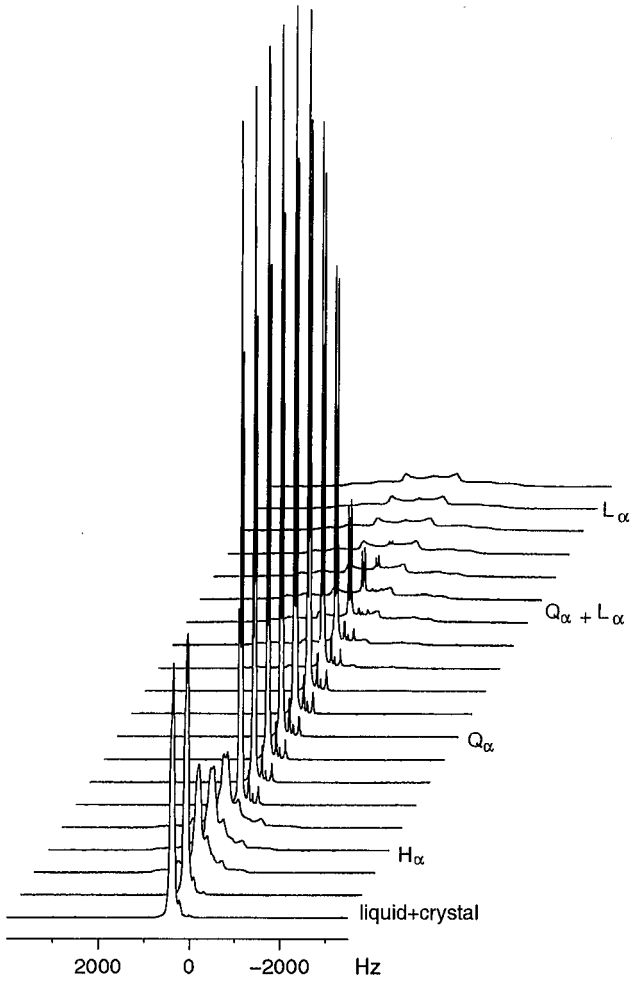

Figure 4. ^2H NMR spectrum of perdeuterated formamide in CTAB78 as a function of temperature from 323 (bottom) to 394 K (top) with a step of 3.5 K.

the temperature range 344−362 K CTAB78 has a pure cubic phase, the symmetry of which results in a vanishing average NQCC; hence, the NMR spectrum displays singlets. At the temperatures 362−380 K, both lamellar and cubic phases are likely to coexist. According to Doane *et al.*,[23] the average

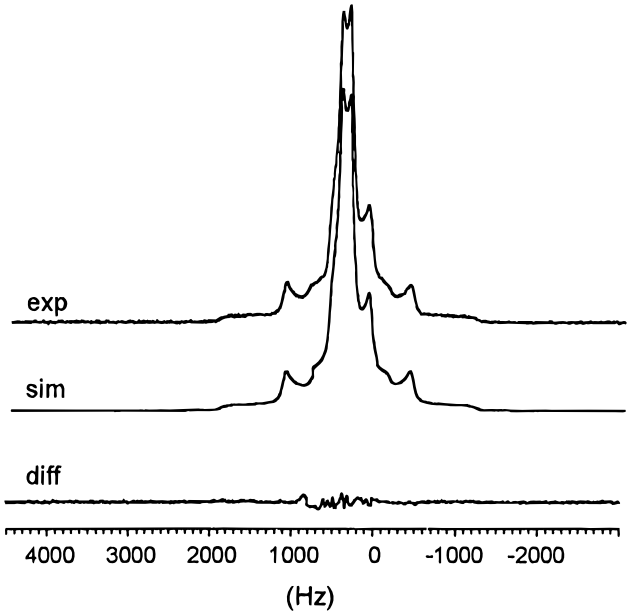

Figure 5. Experimental and simulated ^{2}H NMR spectrum of perdeuterated formamide in CTAB78 and their difference at 341 K.

NQCC of the surfactant molecule in the lamellar phase is −2 times the one in the hexagonal phase in the fast-motion regime. Therefore, the observed ^{14}N quadrupolar splitting of CTAB is doubled as compared to the one in the hexagonal phase (Figure 3). The proportion of the lamellar phase increases at the cost of the cubic phase with increasing temperature (Figure 4). Finally, above 380 K a pure lamellar phase exists in CTAB78.

Similar phase behavior for CTAB78 was also seen in the ^{131}Xe NMR study.[6] The phase boundaries are shifted (because of dissolved xenon gas[6]) with respect to those observed in the X-ray diffraction experiment for pure CTAB/FA,[1] resulting in the cubic phase existing only in the narrow temperature range. The coexistence of the cubic and lamellar phases may be due to slight concentration and/or temperature gradients.

Line Shape of Formamide. The NMR line shape under quadrupolar interaction in the fast motion regime reveals the distribution of the Euler angles that specify the orientations of the average EFG tensor. For CTAB78, the ^{2}H NMR spectrum of oriented FA-d_3 is well-modeled by a superposition of symmetric powder patterns in both lamellar and hexagonal phases. The powder pattern arises most likely from FA, moving in the randomly oriented domains of uniaxial mesophases, where $\bar{\eta}_D$ vanishes. The existence of such domains is possible, if the anisotropy of the diamagnetic susceptibility of the mesophase is small enough to cause incomplete orientation of the molecules along the external magnetic field in the viscous solution. A typical fit of a ^{2}H NMR spectrum corresponding to the hexagonal phase is shown in Figure 5.

Figure 6a displays the ^{2}H NMR spectrum of FA-d_3 in CTAB60 at 340 K before heating the sample to the isotropic phase. It shows a superposition of three symmetric powder patterns, but in this case all of the orientations of **n** are not equally probable. To model the spectrum, eq 3 has to be convoluted with the Lorentzian line shape and the distribution function of θ_D has to be determined. We have assumed the same Gaussian distribution for all θ_D, defined by the mean value θ_0 and the standard deviation $\Delta\theta$ (Figure 6a). The resulting line shape fit is shown in Figure 6a, where θ_0 is chosen to be 90° and the value $\Delta\theta = 20.5°$ results from the fit. The reason for the nonuniform distribution of θ_D in the ^{2}H NMR spectra of CTAB60 is probably the macroscopic character of the domains, which results in the distribution of director orientation.

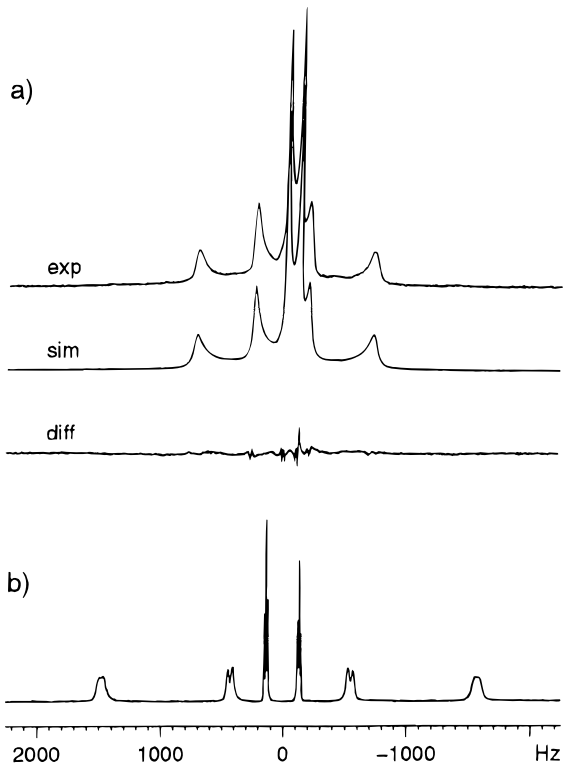

Figure 6. (a) Experimental and simulated ^{2}H NMR spectrum of perdeuterated formamide in CTAB60 and their difference at 340 K before heating the sample to the isotropic phase. In the simulated spectrum the Gaussian distribution, $P(\theta_D) = 1/((2\pi)^{1/2}\Delta\theta)\exp\{-[(\theta_D - \theta_0)/\Delta\theta]^2/2\}$, for θ_D has been used. (b) Experimental ^{2}H NMR spectrum of CTAB60 at 340 K after the sample was heated to the isotropic phase and subsequently cooled back in the magnet.

Figure 6b shows the ^{2}H NMR spectrum of CTAB60 after the sample had been heated to the isotropic phase and subsequently cooled to 340 K. A dramatic change is seen as compared to Figure 6a. The quadrupolar splittings are the same as before, but the mean angle θ_0 has changed from 90° to 0°, which means that the mean orientation of **n** has turned from perpendicular to parallel with respect to the external magnetic field. Also the distribution function of θ_D is very sharp, resulting in the improved resolution. Consequently, the spectrum shows some fine structure due to the spin−spin and dipolar couplings. The ^{14}N NMR spectra of FA and CTAB in CTAB60 show the corresponding change in the director orientation. These changes can be rationalized by the decreased viscosity of CTAB60 when the oriented phase is approached from the isotropic phase, which allows the torque due to the magnetic field acting on the anisotropy of the diamagnetic susceptibility to turn the domains parallel.

First Principles Results. The computed ^{2}H and ^{14}N NQCCs in FA and the corresponding asymmetry parameters $\eta_i = (F_{aa}^i - F_{bb}^i)/F_{cc}^i$ are collected in Table 1, where some reference values are also given. One should note that in our results the principal values F_{kk}^i ($k = a, b, c$) are ordered according to increasing absolute value.

The HIV basis is considered generally to be close to the basis set limit in NMR properties.[17] ^{2}H and ^{14}N quadrupolar couplings decrease, however, by up to 5% on improving from the HIII level.[21] From the comparison of the uncorrelated SCF results with the relatively well-correlated CCD ones, it is apparent that the deuteron NQCCs change very little upon introduction of electron correlation. On the contrary, the nitrogen NQCC is significantly reduced (in absolute magnitude) at the same time. The CCD values in Table 1 represent the

TABLE 1: Theoretical Nuclear Quadrupolar Coupling Constants (kHz) and Asymmetry Parameters for the ^{2}H and ^{14}N Nuclei in Formamide[a]

method	basis	energy/Ha	χ_N	η_N	χ_{D_1}	η_{D_1}	χ_{D_2}	η_{D_2}	χ_{D_3}	η_{D_3}
SCF	HIV	−169.013601	−4451	−0.023	183	−0.037	282	−0.204	280	−0.178
CCD	HIV	−169.766641	−4173	−0.023	183	−0.053	284	−0.185	282	−0.161
BPW91	HIV	−169.965515	−4065	−0.043	182	−0.067	281	−0.169	279	−0.147
SCF[b]	TZV*p*		−4530	0.014						
SCF[c]	6-31G*		−3882	0.028	182	0.036	292	0.188	287	0.173
cluster model[c]			−2941	0.394	182	0.038	221	0.223	285	0.147
microwave[d]			−3848	0.019						
microwave[e]			−3852	0.028						
NMR T_1 in neat liquid[f]			−2840		170		250		250	
$CH_3(CH_2)_2N(CH_3)_3Br$:										
BPW91	HIII	−2867.368056	315	0.106						

[a] Results from calculations and experiments from other groups are also given for comparison. Corresponding ^{14}N data for the CTAB model are given. For the labeling of the nuclei, see Figure 7. [b] Reference 24. [c] Reference 25. [d] Reference 9. [e] Reference 10. [f] Reference 5.

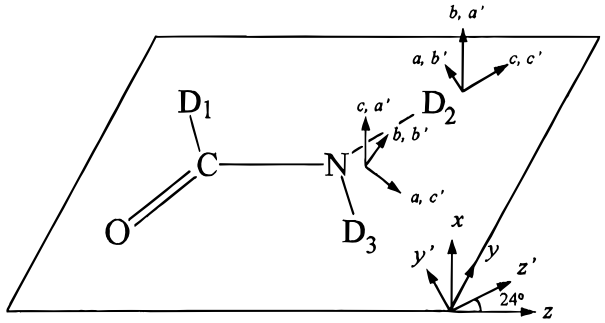

Figure 7. Molecule-fixed axes (x, y, z) and (x', y', z'), where the latter is the principal axis system of the orientation tensor of formamide. The principal axis systems (a, b, c) and (a', b', c') of the EFG tensors in formamide, the first set in the order of increasing magnitude and then the second one with a' perpendicular and b', c' in the molecular plane.

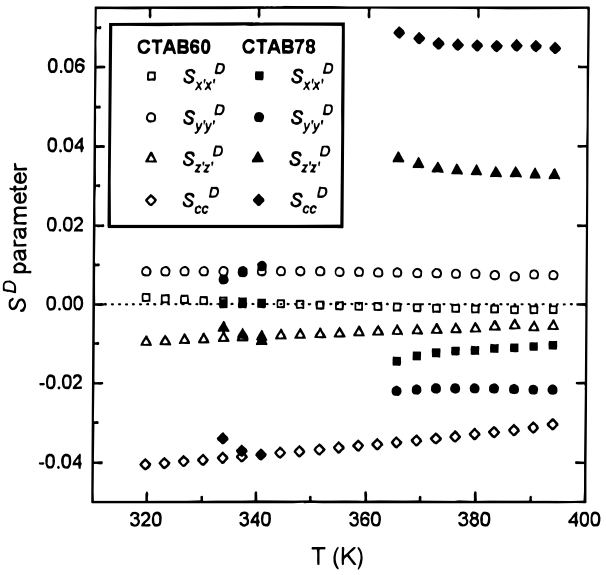

Figure 8. Orientational order parameters, $S_{x'x'}{}^D$, $S_{y'y'}{}^D$, and $S_{z'z'}{}^D$ of formamide and $S_{cc}{}^D$ of CTAB, as a function of temperature in CTAB60 and CTAB78.

dynamical correlation limit in the dilute gas phase ^{2}H and ^{14}N NQCCs of FA, based on a series of calculations where correlation treatment is systematically improved, as will be discussed elsewhere.[21]

DFT provides another approach to the many-electron problem. The BPW91 results for the χ_D's are slightly below those of the CCD calculation. In the χ_N case the difference is bigger, about 2.6%. The asymmetries of the NQCCs are generally small, with the largest values being those of the amide group deuterons.

Comparing with the gas phase experimental values that are available for nitrogen, the computed values are 5.6% (BPW91) and 8.4% (CCD) higher than the ones by microwave spectroscopy. The calculated values correspond to a rigid molecule, which may be a dubious approximation as the amide group has low-energy vibrational modes associated with it.

The PAS of the $F_{\alpha\beta}$ tensors for ^{14}N of FA is oriented so that the c axis is always perpendicular to the plane of the molecule and the a axis makes the angle −37.1° (CCD) or −21.6° (BPW91) with the $\overline{CN}$ vector (Figure 7). The axis c for the ^{2}H tensors is always very close (within 0.5°) to the direction of the associated bond. Axis b is perpendicular to the molecular plane.

On entering the liquid phase, the NQCCs are seen to change. Firstly, $|\chi_N|$ reported in ref 5 is reduced by about 1 MHz from the gas phase value. The D_1 deuteron (associated with the carbonyl group) has its NQCC reduced by about 6% and the D_2 deuteron (*trans* to oxygen in FA) by 18% in the neat liquid FA. The latter change is due to the preferential geometry of association of successive FA molecules in the hydrogen bond network of the neat liquid.[5] The cluster model of ref 25 is in a relatively good agreement with the experiments by the same group.[5] The model, based on SCF calculations of FA clusters of increasing sizes, obviously correctly reproduces the principal medium effects.

The optimized geometry for the $CH_3(CH_2)_2N(CH_3)_3Br$ fragment is displayed in Figure 2. χ_N for the polar head-group of CTAB is given in Table 1, together with the corresponding asymmetry parameter. It is seen that the NQCC is very small due to the highly symmetric nature of the nitrogen site in CTAB. Although the HIII basis set is not fully converged for EFG calculations, the obtained χ_N (315 kHz) provides a reasonable estimate. The principal axis c of the EFG tensor is collinear with the C−N−Br fragment.

Orientation. There is only one nitrogen atom in CTAB and thus only one measured ^{14}N quadrupolar splitting. Therefore, the orientation tensor for the polar head-group of CTAB can be calculated only if the assumptions in eq 5 are valid. Our calculation with the static model of CTAB yields a small η. However, averaging over intramolecular motion results in cylindrically symmetric EFG tensor. The orientation parameter $S_{cc}{}^D$ of the polar head-group of CTAB can be, consequently, calculated from eq 5. The measurement yields only the absolute value of the ^{14}N quadrupolar splitting, but the sign of $S_{cc}{}^D$ can be chosen on the basis that **n** is parallel with the long axis of the CTAB molecule in the lamellar phase and perpendicular to it in the hexagonal phase. The values obtained are shown in Figure 8. The ratio between the values of $S_{cc}{}^D$ in the lamellar and hexagonal phases is near −2, as was that for the corresponding quadrupolar splittings discussed earlier.

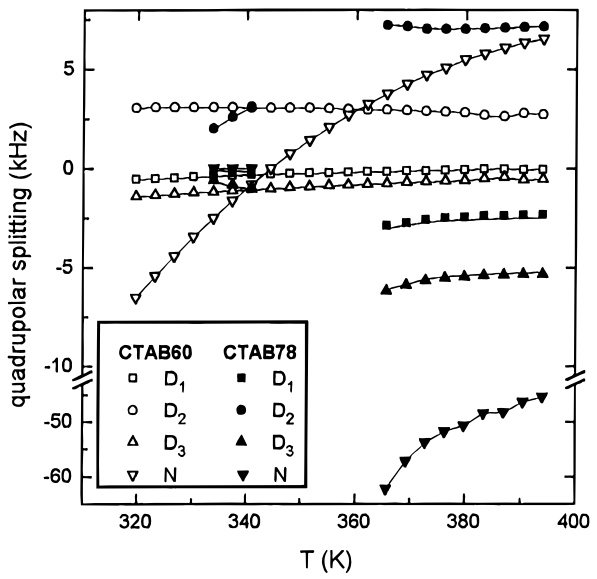

Figure 9. Experimental and fitted quadrupolar splittings of formamide in CTAB60 and CTAB78. Quadrupolar coupling constants have been taken from the neat liquid experiments.[5]

The orientation of a planar molecule in a uniaxial environment can be described with three orientational order parameters, S_{zz}^D, $(S_{xx}^D - S_{yy}^D)$ and S_{yz}^D, where the molecule-fixed coordinate system is chosen as in Figure 7. Then

$$\overline{\chi_i} = \frac{-2eQ_i}{3h}\{[l_{zb'}{}^2F_{b'b'}{}^i + l_{zc'}{}^2F_{c'c'}{}^i - {}^1/_2(F_{a'a'}{}^i + l_{yb'}{}^2F_{b'b'}{}^i + l_{yc'}{}^2F_{c'c'}{}^i)]S_{zz}{}^D + {}^1/_2(F_{a'a'}{}^i - l_{yb'}{}^2F_{b'b'}{}^i - l_{yc'}{}^2F_{c'c'}{}^i) \times (S_{xx}{}^D - S_{yy}{}^D) + (l_{yb'}l_{zb'}F_{b'b'}{}^i + l_{yc'}l_{zc'}F_{c'c'}{}^i)S_{yz}{}^D\} \quad (6)$$

where F_{jj}^i are the elements of the EFG tensor in its PAS ($j = a', b', c'; a'$ perpendicular to and b', c' in the molecule plane, Figure 7). $l_{\alpha j}$ is the direction cosine between the molecule-fixed coordinate axis α and the principal axis j.

Four different values of the quadrupolar splittings are obtained from the ^{2}H and ^{14}N NMR spectra of FA. To obtain the three S^D tensor elements of FA, the experimental NQCCs in the neat liquid, where the asymmetry parameters were assumed to be zero,[5] were utilized. The values were assumed to be independent of temperature in the range considered, and they were extracted from Figures 8 and 9 of ref 5. Also theoretical CCD results (Table 1) were used to find out the sensitivity of the orientation parameters to the choice of NQCCs corresponding to different media. For the calculation of the quadrupolar coupling tensor elements in the (x, y, z) frame, the microwave structure[12] was, again, chosen. The assignment of deuteriums was done on the basis of the chemical shifts,[26] $\delta(D_1) > \delta(D_2) \geq \delta(D_3)$, which leads to the order of quadrupolar splittings of $|\nu_Q(D_2)| > |\nu_Q(D_3)| > |\nu_Q(D_1)|$. Because only the absolute values of the quadrupolar splittings are obtained from the spectra, all of the 16 possible sign combinations have to be taken into consideration. To obtain the correct combination, least-squares fits were made with all of the eight independent combinations. Figure 9 displays the best results, in which only the relative signs are meaningful.

Better fits were obtained by using the NQCC values of FA corresponding to the liquid phase[5] rather than the ones corresponding to the gas phase. Particularly in the latter the larger value (147%) of the theoretical ^{14}N NQCC compared to the former causes the failure of the fit. Earlier investigations[27,28] indicate that FA is found in two environments in the micellar solutions of CTAB: (a) bound in the polar outer layer of the micelle and (b) situated as a free solvent layer between the micelles. The dimensions of both environments are of the same order of magnitude, as the thicknesses of layers are about 4 and 6 Å in CTAB60 for the bound and free FA, respectively.[1] Hydrogen bonding has been shown to have a large effect on the EFG tensor values of FA.[25] Therefore, the EFG tensors of FA are expected to change on the surface of the micelle, where the hydrogen bonding between FA molecules is disturbed and the negative counterions (Br^-) may form complexes with FA. Nevertheless, the fact that the EFG tensor values of the neat liquid are well-fitted in the present study may indicate that FA appears mostly as a free solvent.

As a result of the least-squares fits, the orientational order parameters of FA, S_{zz}^D, $(S_{xx}^D - S_{yy}^D)$ and S_{yz}^D, are obtained. The out-of-plane orientation tensor element S_{xx}^D is dominantly determined by the ^{14}N quadrupolar splittings of FA and the in-plane orientation tensor elements S_{yy}^D, S_{zz}^D, and S_{yz}^D by the ^{2}H quadrupolar splittings of FA in the fit. Only the absolute values and the relative signs of the three orientation parameters are known. However, some speculative conclusions may be drawn from the average orientation of FA.

The PAS of the $S_{\alpha\beta}^D$ tensor is obtained by rotating the molecule-fixed frame around the x-axis (Figure 7). Resulting orientation tensor elements for CTAB60 and CTAB78 are shown in Figure 8, based on the data fitted with the liquid phase NQCCs. The orientation of PAS is independent (within 1.5°) of temperature and phase. For CTAB78 in the lamellar phase, the absolute value of $S_{z'z'}^D$ is the largest and the other two are opposite in sign and about half of the magnitude of $S_{z'z'}^D$. A positive $S_{z'z'}^D$ indicates that the z'-axis prefers parallel orientation with **n**, whereas the negative one indicates perpendicular orientation. In the former case, the z'-axis of FA prefers perpendicular orientation on average and in the latter parallel orientation with respect to the surface of the micelle. The facts that the oxygen atom in FA has a negative charge and that it is expected to repel the negative counterions Br^- support the idea that the perpendicular orientation of the z'-axis with respect to the surface of the micelle is the most favorable one.

The PAS of $S_{\alpha\beta}^D$ in the hexagonal phase is the same as in the lamellar one, indicating that the surface of the micelle orients FA similarly in the two phases. The orientation parameter of the surface of the micelle, S_{cc}^D, was scaled by $-{}^1/_2$ in the hexagonal phase as compared to the lamellar one. That kind of scaling is not seen in the orientation parameters of FA. The FA molecules may diffuse from one micelle to another, which makes the assumptions of Doane *et al.*[23] inapplicable in this case.

Conclusions

We have studied two different CTAB/formamide mixtures within a wide temperature range by ^{2}H and ^{14}N NMR spectroscopy. On the basis of the ^{14}N NMR spectra of CTAB, the observed phases have been identified. The phase order is liquid + crystal → hexagonal → isotropic and liquid + crystal → hexagonal → cubic → cubic + lamellar → lamellar in the order of increasing temperature for CTAB60 and CTAB78, respectively. For CTAB60, the observed mesophase corresponds to the earlier observations;[1,2] however, the isotropic phase has not been observed before. For CTAB78, the existence of three different mesophases agrees with our earlier ^{129}Xe and ^{131}Xe NMR observations.[6] The phase transition temperatures of the present samples are shifted with respect to pure CTAB/FA systems because of xenon gas dissolved.

The line shape analysis of the ^{2}H NMR patterns of formamide-d_3 show that the simple model of formamide moving fast

compared to the NQCCs in the uniaxial environment could be used in both samples. Depending on the sample history, different kinds of line shapes are obtained, which is caused by the modified distributions of the liquid crystal domains.

The orientation parameters of CTAB and formamide have been calculated. For that purpose we utilized theoretical values for the ^{14}N NQCC in a model of the polar head-group region of CTAB and ^{2}H and ^{14}N NQCCs of formamide. Since the latter correspond to the gas phase values, the experimental liquid phase values of NQCCs of formamide were chosen.[5] The orientation parameter of CTAB in the lamellar phase is opposite in sign and 2-fold in magnitude as compared to the hexagonal phase value. The liquid phase NQCC values of formamide fit excellently to the measured quadrupolar splittings, which may indicate that formamide molecules appear mostly as a free solvent rather than bound into the surface of the micelle. The orientation parameter values of formamide indicate that the PAS z'-axis of the formamide molecule is oriented either perpendicular to or parallel with the surface of the micelle. The former case is thought to be more likely on the basis of the repulsion between the negative counterions and the negatively charged oxygen in formamide.

Acknowledgment. The authors are grateful to the Academy of Finland and the Neste Foundation for financial support. J.V. thanks the Vilho, Yrjö, and Kalle Väisälä Fund for a grant. Center for Scientific Computing (CSC, Espoo, Finland) provided with the computational facilities.

References and Notes

(1) Auvray, X.; Petipas, C.; Anthore, R.; Rico, I.; Lattes, A. *J. Phys. Chem.* **1989**, *93*, 7458.

(2) Belmajdoub, A.; Marchal, J. B.; Canet, D.; Rico, I.; Lattes, A. *New. J. Chem.* **1987**, *11*, 415.

(3) Wittebort, R. J.; Olejniczak, E. T.; Griffin, R. G. *J. Chem. Phys.* **1987**, *86*, 5411.

(4) Hirschinger, J.; English, A. D. *J. Magn. Reson.* **1989**, *85*, 542.

(5) Ludwig, R.; Bohmann, J.; Farrar, T. C. *J. Phys. Chem.* **1995**, *99*, 9681.

(6) Ylihautala, M.; Ingman, P.; Jokisaari, J.; Diehl, P. *Appl. Spectrosc.*, in press.

(7) Massiot, D.; Thiele, H.; Müller, D. *WINFIT program (for Windows)*; CNRS, Bruker Analytische Messtechnik, and Bruker-Franzen: Orleans, France, Karlsruhe, Germany, and Bremen, Germany, 1995.

(8) Press, W. H.; Teukolsky, S. A.; Vetterling, W. T.; Flannery, B. P. *Numerical Recipes, The Art of Scientific Computing*, 2nd ed.; Cambridge University Press: Cambridge, U.K., 1992; Chapter 15.

(9) Kukolich, S. G.; Nelson, A. C. *Chem. Phys. Lett.* **1971**, *11*, 383.

(10) Kirchhoff, W. H.; Johnson D. R. *J. Mol. Spectrosc.* **1973**, *45*, 159.

(11) Parr, R. G.; Yang, W. *Density-Functional Theory of Atoms and Molecules*; Oxford University Press: Oxford, U.K., 1989.

(12) Hirota, E.; Sugisaki, R.; Nielsen, C. J.; Sørensen, G. O. *J. Mol. Spectrosc.* **1974**, *49*, 251.

(13) Becke, A. D. *Phys. Rev.* **1988**, *A38*, 3098.

(14) Perdew, J. P.; Wang, Y. *Phys. Rev.* **1991**, *B45*, 13244.

(15) Ruud, K.; Helgaker, T.; Kobayashi, R.; Jørgensen, P.; Bak, K. L.; Jensen, H. J. Aa. *J. Chem. Phys.* **1994**, *100*, 8178.

(16) Barszczewicz, A.; Helgaker, T.; Jaszunski, M.; Jørgensen, P.; Ruud, K. *J. Chem. Phys.* **1994**, *101*, 6822.

(17) Jaszunski, M.; Szymanski, S.; Christiansen, O.; Jørgensen, P.; Helgaker T.; Ruud, K. *Chem. Phys. Lett.* **1995**, *243*, 144.

(18) Vosko, S. H.; Wilk, L.; Nusair, M. *Can. J. Phys.* **1980**, *58*, 1200.

(19) Pyykkö, P.; Li, J. *Report HUKI 1-92*, Department of Chemistry, University of Helsinki: Helsinki, Finland, 1992.

(20) Frisch, M. J.; Trucks, G. W.; Schlegel, H. B.; Gill, P. M. W.; Johnson, B. G.; Robb, M. A.; Cheeseman, J. R.; Keith, T.; Petersson, G. A.; Montgomery, J. A.; Raghavachari, K.; Al-Laham, M. A.; Zakrzewski, V. G.; Ortiz, J. V.; Foresman, J. B.; Cioslowski, J.; Stefanov, B. B.; Nanayakkara, A.; Challacombe, M.; Peng, C. Y.; Ayala, P. Y.; Chen, W.; Wong, M. W.; Andres, J. L.; Replogle, E. S.; Gomperts, R.; Martin, R. L.; Fox, D. J.; Binkley, J. S.; Defrees, D. J.; Baker, J.; Stewart, J. P.; Head-Gordon, M.; Gonzalez, C.; Pople, J. A. *Gaussian 94, Revision B.1*; Gaussian, Inc.: Pittsburgh, PA, 1995.

(21) Vaara, J.; Kaski, J.; Jokisaari, J.; Diehl, P. Manuscript in preparation.

(22) Hoatson, G. L.; Vold, R. L. In *NMR Basic Principles and Progress, Solid-State NMR III*; Diehl, P., Günther, H., Kosfeld, R., Seelig, J., Blümich, B., Eds.; Springer-Verlag: Berlin, 1994; Vol. 32.

(23) Chidichmo, G.; Vaz, N. A. P.; Yaniv, Z.; Doane, J. W. *Phys. Rev. Lett.* **1982**, *49*, 1950.

(24) Palmer, M. P. *Chem. Phys.* **1988**, *127*, 335.

(25) Ludwig, R.; Weinhold, F.; Farrar, T. C. *J. Chem. Phys.* **1995**, *102*, 5118.

(26) Sørensen, O. W.; Schebye, S.; Lawesson, S.-O.; Jakobsen, H. J. *Org. Magn. Reson.* **1981**, *16*, 322.

(27) Belmajdoub, A.; Boubel, J. C.; Canet, D. *J. Phys. Chem.* **1989**, *93*, 4844.

(28) Perche, T.; Auvray, X.; Petipas, C.; Anthore, R.; Rico, I; Lattes, A.; Bellissent, M. C. *J. Phys. I Fr.* **1992**, *2*, 923.